NASA/TM-2000-209027

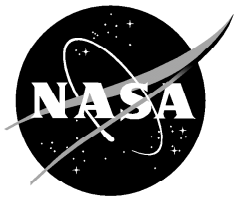

Visualization of In-Flight Flow Phenomena Using Infrared Thermography

D. W. Banks
NASA Dryden Flight Research Center
Edwards, California

C. P. van Dam and H. J. Shiu
Department of Mechanical and Aeronautical Engineering
University of California, Davis
Davis, California

G. M. Miller
PVP Advanced EO Systems
Orange, California

July 2000

The NASA STI Program Office…in Profile

Since its founding, NASA has been dedicated to the advancement of aeronautics and space science. The NASA Scientific and Technical Information (STI) Program Office plays a key part in helping NASA maintain this important role.

The NASA STI Program Office is operated by Langley Research Center, the lead center for NASA's scientific and technical information. The NASA STI Program Office provides access to the NASA STI Database, the largest collection of aeronautical and space science STI in the world. The Program Office is also NASA's institutional mechanism for disseminating the results of its research and development activities. These results are published by NASA in the NASA STI Report Series, which includes the following report types:

- TECHNICAL PUBLICATION. Reports of completed research or a major significant phase of research that present the results of NASA programs and include extensive data or theoretical analysis. Includes compilations of significant scientific and technical data and information deemed to be of continuing reference value. NASA's counterpart of peer-reviewed formal professional papers but has less stringent limitations on manuscript length and extent of graphic presentations.

- TECHNICAL MEMORANDUM. Scientific and technical findings that are preliminary or of specialized interest, e.g., quick release reports, working papers, and bibliographies that contain minimal annotation. Does not contain extensive analysis.

- CONTRACTOR REPORT. Scientific and technical findings by NASA-sponsored contractors and grantees.

- CONFERENCE PUBLICATION. Collected papers from scientific and technical conferences, symposia, seminars, or other meetings sponsored or cosponsored by NASA.

- SPECIAL PUBLICATION. Scientific, technical, or historical information from NASA programs, projects, and mission, often concerned with subjects having substantial public interest.

- TECHNICAL TRANSLATION. English-language translations of foreign scientific and technical material pertinent to NASA's mission.

Specialized services that complement the STI Program Office's diverse offerings include creating custom thesauri, building customized databases, organizing and publishing research results…even providing videos.

For more information about the NASA STI Program Office, see the following:

- Access the NASA STI Program Home Page at ***http://www.sti.nasa.gov***

- E-mail your question via the Internet to help@sti.nasa.gov

- Fax your question to the NASA Access Help Desk at (301) 621-0134

- Telephone the NASA Access Help Desk at (301) 621-0390

- Write to:
  NASA Access Help Desk
  NASA Center for AeroSpace Information
  7121 Standard Drive
  Hanover, MD 21076-1320

NASA/TM-2000-209027

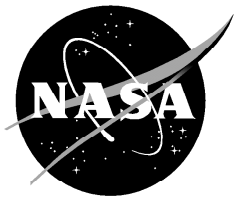

Visualization of In-Flight Flow Phenomena Using Infrared Thermography

D. W. Banks
NASA Dryden Flight Research Center
Edwards, California

C. P. van Dam and H. J. Shiu
Department of Mechanical and Aeronautical Engineering
University of California, Davis
Davis, California

G. M. Miller
PVP Advanced EO Systems
Orange, California

National Aeronautics and
Space Administration

Dryden Flight Research Center
Edwards, California 93523-0273

July 2000

Visualization of In-Flight Flow Phenomena Using Infrared Thermography

D. W. Banks,[1] C. P. van Dam,[2] H. J. Shiu,[3] and G. M. Miller[4]

Keywords: Infrared thermography, boundary layer transition, shock waves, supersonic flow

ABSTRACT

Infrared thermography was used to obtain data on the state of the boundary layer of a natural laminar flow airfoil in supersonic flight. In addition to the laminar-to-turbulent transition boundary, the infrared camera was able to detect shock waves and present a time dependent view of the flow field. A time dependent heat transfer code was developed to predict temperature distributions on the test subject and any necessary surface treatment. A commercially available infrared camera was adapted for airborne use in this application. Readily available infrared technology has the capability to provide detailed visualization of various flow phenomena in subsonic to hypersonic flight regimes.

1 INTRODUCTION

The use of infrared (IR) thermography to visualize certain flow phenomena is not new. Infrared technology has been employed in wind tunnels [1] and in flight at subsonic to hypersonic conditions with both local (that is, when the camera and subject surface are on one aircraft) [2,3,4] and remote camera installations [5,6,7]. However, with state-of-the-art equipment and advanced methods, greater success and improved resolution of details of various flow phenomena has become possible. Infrared thermography has many benefits over other methods. It is global in nature and non-intrusive. In general, it does not require the application of any environmentally unfavorable substances. Furthermore, it can be used throughout a flight and over a range of conditions, instead of being limited to solitary test points.

The basic principle behind IR thermography is the measuring of surface emissions in the IR radiation band, that are directly related to surface temperature. Surface shear stress and, thereby, convective heat transfer with the freestream varies with the boundary layer state. This difference in convective heat transfer results in a temperature gradient on the surface where the boundary layer state changes, such as at transition. With state-of-the-art equipment this temperature difference can be measured to an accuracy of nearly 0.1°C over a small area. These characteristics make IR thermography a very powerful tool to visualize certain flow phenomena. In addition to transition, any flow phenomena that create measurable temperature changes can be visualized. These include shock waves and possibly flow separation.

Author(s): *1 Aerodynamics Branch, NASA Dryden Flight Research Center,*
Mail Stop D-2228, Edwards, California 93523, U.S.A.
2,3 Dept. of Mechanical and Aeronautical Engineering, University of California, Davis
One Shields Ave., Davis, California 95616, U.S.A.
4 PVP Advanced EO Systems,
605 N. Poplar, Orange, California 92868, U.S.A.

Corresponding author: D. W. Banks

This paper presents the results of a recent flight investigation of a supersonic natural laminar flow airfoil using infrared thermography.

Use of trade names or names of manufacturers in this document does not constitute an official endorsement of such products or manufacturers, either expressed or implied, by the National Aeronautics and Space Administration.

2 METHODOLOGY AND APPROACH

As with any imaging visualization application, the study of the supersonic natural laminar flow airfoil can be divided into two primary components: the imaging system and the test subject. In this investigation, the imaging system and test subject were mounted on the same aircraft (local).

2.1 The Infrared Imaging System

A digital infrared camera system was designed and mounted on the starboard armament rail of an F-15B aircraft. The IR camera system is shown in Fig. 1. The camera is a Raytheon Radiance HS digital infrared camera. For this first phase of the investigation, the images were stored as analog video on Hi-8 videotape.

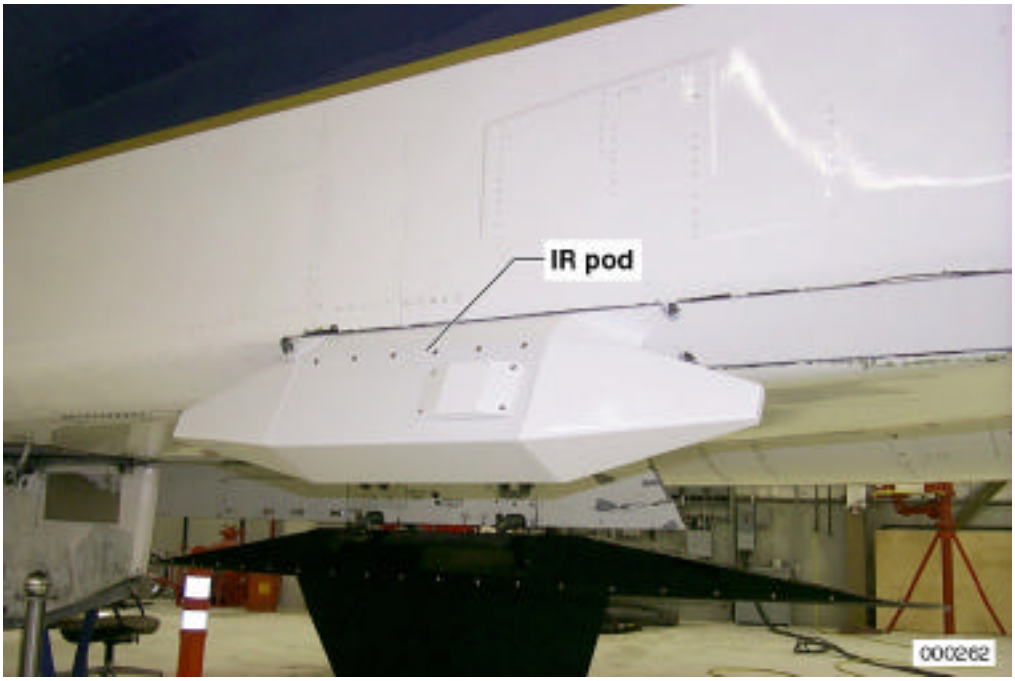

Fig. 1. Infrared camera system mounted on starboard armament rail of NASA F-15B aircraft.

2.1.1 System Background

To explore the feasibility of utilizing an IR imaging system that supports visualization studies, an initial series of tests were conducted using an AN/AAS-38 NITE Hawk (Lockheed Martin) targeting pod mounted on a chase aircraft. The targeting pod, installed on the left side of an F/A-18 aircraft, provided a stabilized infrared imaging capability in the 8- to 12-micron spectral band. Initial data acquired with the system indicated that IR thermography was a very promising tool for flow visualization [6]. The presence of fixed pattern noise and other

residual effects of the scanned image required extensive post processing to minimize the impact on the accuracy of the experimental data.

For the next phase of the investigation, an advanced version of the NITE Hawk targeting pod equipped with a 3- to 5-micron focal plane array sensor was utilized. Experimental results obtained with this sensor indicated improved sensitivity and resolution. The primary limitation of this method was the ability to position the experiment so that the chase aircraft was sufficiently close to the experiment and had a sightline angle that could sufficiently acquire the region of interest.

For the current phase of the investigation, the proven 3- to 5-micron focal plane array sensor was deployed in an externally mounted pod, located on the experimental aircraft with a fixed line of sight, centered on the region of interest.

2.1.2 System Description

The imaging system is based on a Raytheon Radiance HS camera. The camera uses an Indium-Antimonide (InSb) focal plane with a 256 × 256 array of 30-micron pixels. The sensor responds in the 3- to 5-micron spectral range. A 13mm lens was selected to capture a complete view of the experiment with minimal background within the field of view. The imaging system was packaged within a pod mounted to the right side of the F-15 aircraft (Fig. 1).

To minimize the size of the pod and resultant drag, the sensor was oriented parallel to the air-flow. This also placed the line of sight parallel to the experiment. A fold mirror was incorporated in the design to fold the line of sight inboard and down to center on the region of interest (Fig. 2). A silicon window with an antireflection coating optimized for the 3- to 5-micron spectral band was installed on the inner surface of the pod directly in front of the fold mirror.

To further minimize the volume of the pod, the camera electronics were installed in an adjacent aircraft bay with an interface cable connection to the camera head. The electronics package provides simultaneous NTSC (National Television Systems Committee) standards, S-video, and 12-bit digital output. The camera operational settings could be adjusted on the ground prior to flight through an RS-422 computer interface. The system was equipped with test ports and cables to enable external configuration and test support without the need for aircraft power.

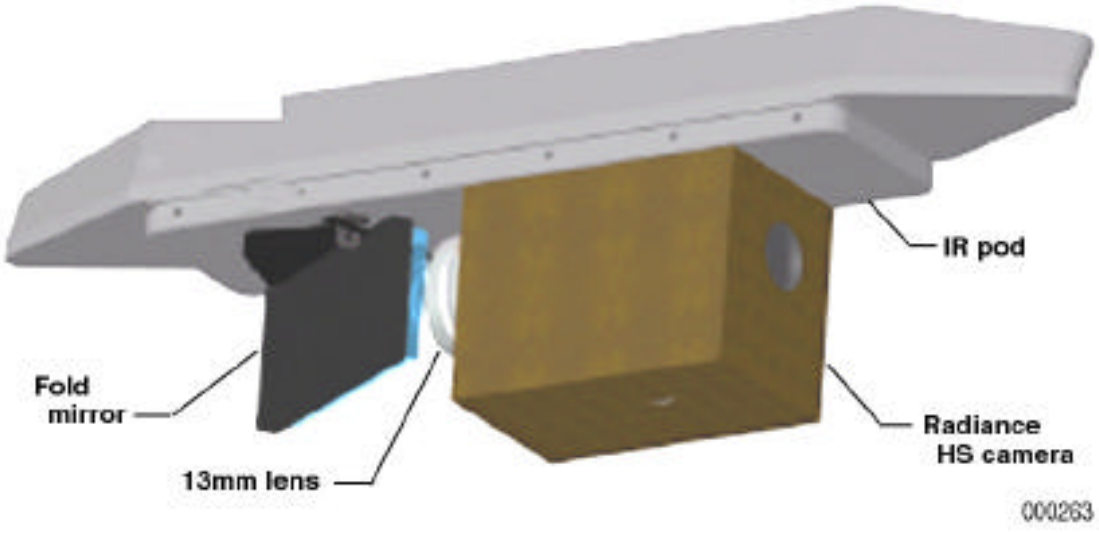

Fig. 2. Infrared camera system inside pod.

2.2 F-15B Test Bed

The NASA F-15B is a two-seat version of the F-15A; a high performance, supersonic, all-weather air-superiority fighter built by McDonnell-Douglas Aircraft Company (now Boeing Aircraft Company). The aircraft is powered by two Pratt & Whitney F100-PW-100 afterburning turbofan engines. The F-15B is 63.7 ft (19.4 m) long with a wingspan of 42.8 ft (13.0 m) and a basic operating weight of 27,500 lbs (122,300 N). The supersonic natural laminar flow test article was mounted on the centerline tank location. The aircraft flight envelope was not limited by the fixture, nor was there significant performance degradation resulting from the test article. The aircraft was outfitted with a flight test nose boom in order to obtain accurate air data during flight.

2.3 The Test Subject

The test article was designed to mount to the centerline store station of the F-15B as shown in Fig. 3. The test article was fabricated out of aluminum 6061-T6. Insulating material was applied over much of the surface to reduce the effects of heat conduction into the test article. The leading and trailing edges were not insulated because of a lack of thickness available in those areas. The insulating material consisted primarily of aluminum impregnated epoxy and syntactic foam. Details on determining the type and amount of insulation applied are discussed in Section 3.

Fig. 3. Supersonic natural laminar flow test article mounted on NASA F-15B aircraft.

3 NUMERICAL PREDICTION OF SURFACE TEMPERATURE

Temperature distribution on the test article was predicted using numerical methods to provide quantitative values for comparison with flight data. The numerical solutions also provided a basis for insulation selection as well as the required temperature range and sensitivity of the infrared imager that was used in this application.

3.1 Methodology

Assuming a wing section with little taper and sweep, the spanwise temperature gradient is small and a two-dimensional model is adequate. The wing is discretized into chordwise and depthwise segments.

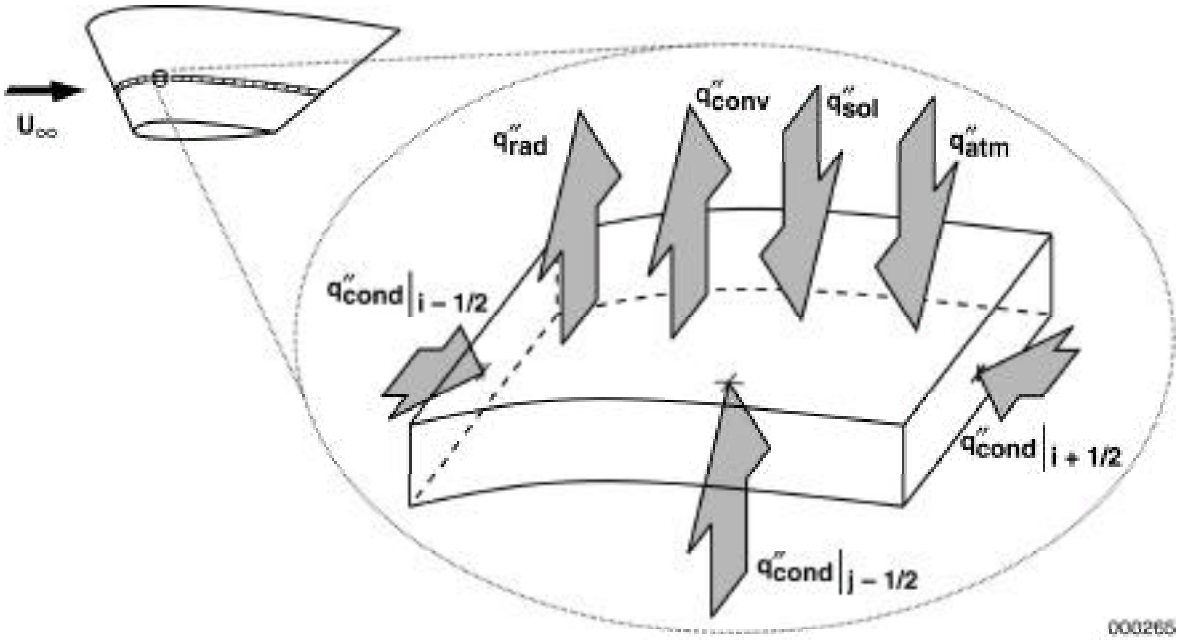

Fig. 4. Heat transfer mechanisms on a wing in flight.

The temperature distribution is determined through heat transfer calculations. Heat transfer is governed by the first and second laws of thermodynamics. For this application, the first law can be expressed as:

$$\frac{\partial}{\partial t}\iiint_V \rho c_p T dV = -\iint_A q'' dA \qquad (1)$$

As illustrated in Fig. 4, there are five significant sources of heat transfer at each wing segment:

$$\frac{\partial}{\partial t}\iiint_V \rho c_{p,skin} T dV = -\iint_A (q''_{conv} + q''_{rad} + q''_{sol} + q''_{atm} + q''_{cond}) dA \qquad (2)$$

q''_{conv} is the convective heat transfer resulting from flow over the wing. The convective heat transfer is dependent on skin friction, as follows:

$$q''_{conv} = \frac{c_f}{2}\rho_\infty U_\infty (T_W - T_{aw})\frac{k}{\mu} \qquad (3)$$

At low Mach numbers, the adiabatic wall temperature is effectively equal to the freestream total temperature. However, as Mach number increases, the recovery factor, R, can make a notable contribution to the adiabatic wall temperature:

$$T_{aw} = T_\infty + R\frac{U_\infty^2}{2c_{p,air}} = T_\infty\left(1 + R\frac{\gamma - 1}{2}M_\infty^2\right) \qquad (4)$$

Because the recovery factor differs in laminar and turbulent boundary layers, the recovery factor influences the surface temperature gradient between laminar and turbulent walls at higher Mach numbers.

q''_{rad} is the heat transfer caused by radiation from the wing surface:

$$q''_{rad} = \varepsilon\sigma T_w^{\,4} \qquad (5)$$

where σ is the Stefan-Boltzmann constant, which relates the maximum possible heat flux radiated by a body to the body's surface temperature. ε is emissivity, a surface property which relates the maximum possible heat flux to the actual heat flux emitted by a body. It is dependent on factors such as material, surface finish, and surface color. Given emissivity, surface temperature distributions can be deduced from radiation measurements such as those performed with infrared detectors.

q''_{sol} is the heat transfer caused by direct solar heating. Currently, q''_{sol} is estimated as a constant value of 1300 W/m^2 when the surface is exposed to the sun. Direct solar heating is assumed to be negligible and is set to zero when the surface is shaded from the sun, as with the test article in this experiment.

q''_{atm} is the diffuse atmospheric heating component radiated from the surrounding atmosphere. As a radiation term, it is expressed similarly to the wing surface radiation component in Equation 4:

$$q''_{atm} = \alpha\sigma T_{\infty}^{4} \qquad [6]$$

In this equation, α is absorptivity, a surface property analogous to emissivity. Absorptivity relates the maximum possible heat flux into a body to the actual heat absorbed by the body.

q''_{cond} is the heat conduction within the wing skin and internal structure. Fourier's law states that:

$$q''_{cond} = -k \quad T \qquad [7]$$

The formulation in Equation 2 was implemented to solve both steady state and time dependent cases. The steady state models were solved iteratively. The time dependent model was solved using the backward Euler method with a time step determined through a solution accuracy requirement [8]. The test article is geometrically symmetric and is assumed to also be thermally symmetric. It is therefore modeled as a half-section with adiabatic conditions at the centerline. The half-section is discretized into 100 chordwise segments and 6 depthwise segments.

Subsonic and transonic skin friction values were numerically determined with MSES, a numerical airfoil development system that can analyze, modify, and optimize airfoils for a wide range of Mach and Reynolds numbers [9]. Supersonic skin friction values were based on the local temperature and calculated by means of linear theory and an empirical two-dimensional flat plate formulation with a compressibility correction [10]. Laminar and turbulent recovery factors were set as follows: $R_{laminar} = 0.85$, $R_{turbulent} = 0.88$ [11]. Atmospheric properties were assumed to be standard.

3.2 Temperature Predictions

Several cases were analytically investigated with thin-skinned and solid-bodied wings at subsonic, transonic, and supersonic conditions through various flight profiles. Sample results and some important conclusions are presented below.

All results indicated the importance of considering heat conduction within the wing structure. Even in cases where the wing surface was modeled as a thin skin with an adiabatic inner surface, chordwise conduction sometimes smears temperature distributions, shifting and weakening the surface temperature gradient between the laminar and turbulent boundary layers.

Fig. 5 shows surface temperature distributions on a wing with transition fixed at 60 percent of chord. In this case, the wing is modeled as solid aluminum, in accordance with the actual test article. Transition location is difficult to discern by inspecting the temperature distribution of the non-insulated wing.

Adding of a thin layer of insulation on the surface can inhibit heat conduction into the wing structure, thereby improving the temperature gradient at the transition location and, consequently, aiding transition detection. Fig. 5 also shows the beneficial effect of adding an insulation layer.

Fig. 5 also reveals the time dependent nature of temperatures at the wing surface. Again, the insulation mitigates the surface conduction effect, improving transition detection by establishing a strong temperature gradient at the transition location.

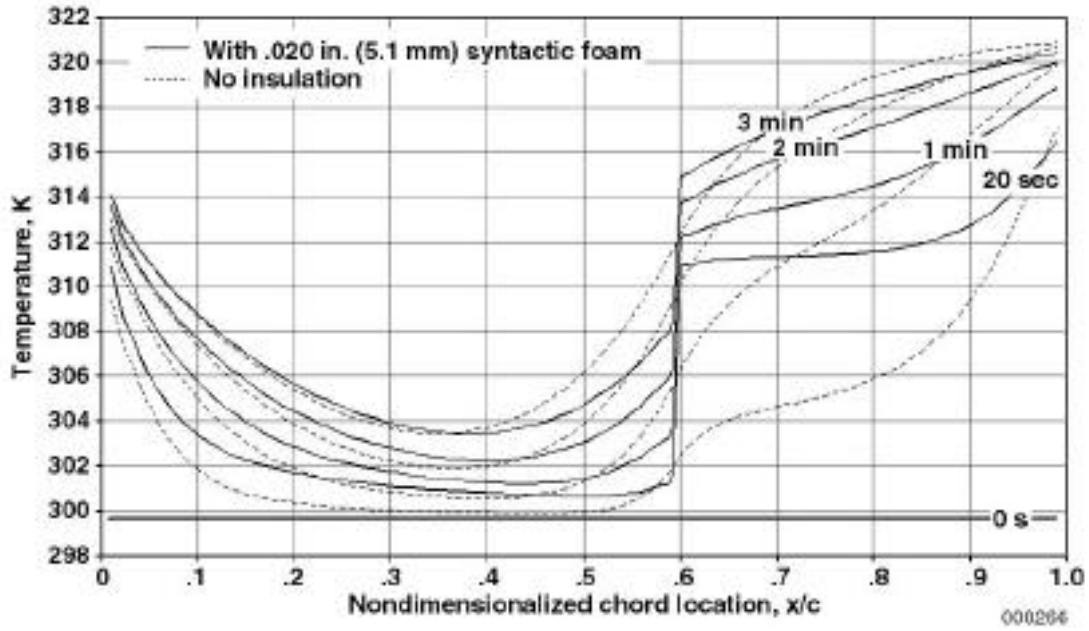

Fig. 5. Temperature distribution history with .020 in. (5.1 mm) syntactic foam. Three percent biconvex airfoil, 3 ft chord, M_∞ = 1.4, 24,500 ft (standard atmosphere), uniform initial temperature of 80 °F (300 K). Transition fixed at 60 percent of chord.

In preparing the test article for investigation of supersonic natural laminar flow, several thicknesses and types of insulation were investigated. Steady state results are shown in Fig. 6. These results and corresponding time dependent solutions show that increased thicknesses of insulation better preserve surface temperature gradients. However, insulation thickness is practically limited by structural constraints. Given the thin test article used in these experiments, a 0.060 in. (15.2 mm) layer of syntactic foam was selected as insulation.

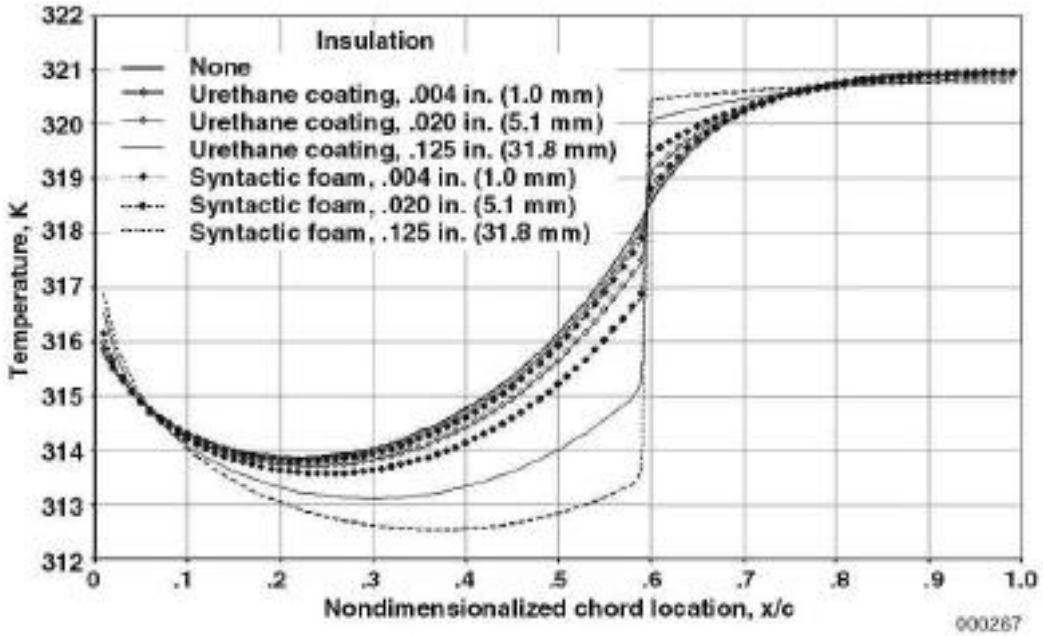

Fig. 6. Steady state surface temperature distributions with insulation. Three percent biconvex airfoil, 3 ft chord, M_∞ = 1.4, 24,500 ft (standard atmosphere). Transition fixed at 60 percent of chord.

4 FLIGHT RESULTS AND DISCUSSION

This paper shows and discusses flow visualization results obtained from flight tests of a natural laminar flow airfoil at supersonic speeds. A natural laminar flow airfoil is designed to maintain large runs of laminar flow without the aid of active devices such as suction. This is usually accomplished largely by wing geometry and surface finish. These visualizations include still and video segments. In addition to the transition boundary, these visualizations were able to capture shock waves impinging on the surface of the test article.

The resultant data was obtained during approximately 10-minute intervals during which the aircraft was accelerated to supersonic speed, held predetermined conditions, and then decelerated back to subsonic speed. The course was selected to optimize the sun angle (minimize or eliminate solar radiation on the test article and avoid reflections back to the camera) for the IR imaging while staying within the supersonic test corridor. Flights were conducted up to Mach 2.0 and up to an altitude of 45,000 ft (13,700 m). The wing geometry (biconvex cross-section) and the physics of supersonic flow allow a favorable pressure gradient to be maintained on the surface from leading to trailing edge. Further in this speed range ($1.0 \leq M \leq 2.0$) there is a reduction in the boundary layer disturbances and reduced leading-edge sweep minimizes crossflow disturbances. This allows a laminar boundary layer to be maintained over a large percentage of the surface at these speeds. The laminar flow is typically terminated (transition occurs) by an impinging shock wave or by the eventual growth of the disturbances (first mode Tollmien-Schlichting [12]) in the boundary layer. It is speculated that the shock wave that caused transition in many images was generated by the camera pod.

Images of the natural laminar flow test article at supersonic flight conditions are shown in Fig. 7. For these cold (relative to adiabatic) wall conditions the cooler dark areas indicate laminar flow and the warmer white areas indicate turbulent flow. This is caused by the higher heating rates (convective) of the surface below the turbulent boundary layer as compared to the laminar boundary layer. The extent of the laminar flow at these supersonic speeds is clearly evident in the figures. The four circular marks in the image are tooling holes in the aluminum beneath the insulating layer. This demonstrates the ability of the camera to discern very small temperature differences. The thin strip at the leading- and trailing-edges were areas that were not insulated as a result of the lack of thickness available to install the insulating material.

Video images are able to reveal additional detail and show time dependent processes within the flow field. As conditions become more severe (higher Reynolds number or strong shock wave) the breakdown of the laminar boundary layer flow can be observed as well as identifying the responsible mechanism in many cases (shock, etc.).

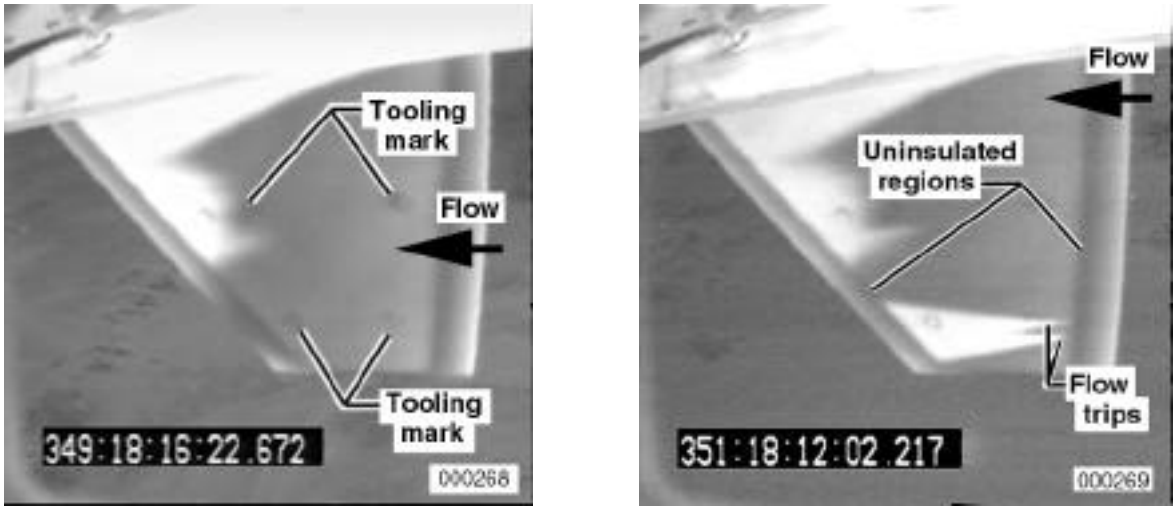

Fig. 7(a). With smooth surface. **Fig. 7(b). With boundary-layer trips.**

Fig. 7. Supersonic natural laminar flow test article.

The flight shown in Fig. 7(b) repeated the profile, but two cylindrical flow trips were attached to the test article. These trips were approximately 0.25 in. (63.5 mm) in diameter and 0.010 in. (2.5 mm) high. This size was calculated to be just above the critical disturbance size for these conditions [13]. The image is shown in Fig. 7(b). Evident in this figure are the transition wedges propagating aft of the trips. Note the good agreement between these two images which were acquired during two separate flights at nearly identical flight conditions. The only difference between Fig. 7(a) and 7(b) being the two boundary-layer trips (and the resulting turbulent wedges). Otherwise, the wing was not altered nor cleaned. This excellent repeatability of the transition phenomena provides further evidence of the maintainability of supersonic natural laminar flow.

Shock waves also cause a measurable change in heating where they impinge the surface and can be visualized by IR thermography, although not as evident as the transition front previously discussed. In Fig. 8 a shock is clearly visible and causes transition at approximately mid-chord. Although the sensors are capable of measuring 0.1°C, as a result of losses (optics, etc.) a slightly higher temperature difference is required.

Finally in Fig. 9 an image obtained at warm (relative to adiabatic) wall conditions at the end of the supersonic run is shown. Now turbulent flow is marked by the cooler dark areas and laminar flow by the warmer white areas. At these lower Mach conditions the higher cooling rates of the surface below the turbulent boundary layer leads to cooler surface temperatures. Also at these conditions the extent of the laminar flow at supersonic speeds is again clearly evident in the figure.

Although the current study was focused on the identification of supersonic boundary layer transition, transition at subsonic speeds were also observed. Previous studies at subsonic speeds employed some method to create heat flux at the surface which was not needed at supersonic speeds. During the deceleration from the supersonic runs the test article was much warmer because of heating during supersonic speeds, which produced the needed heat flux to observe transition at the subsonic speeds similar to what was seen at low supersonic speeds in Fig. 9.

The primary purpose of this early test was to locate boundary layer transition and thus determine the extent of laminar flow attained by this wing design at these supersonic conditions. Additional data shows the progression (time dependence) of the transition front, location of shock waves, and relative temperature of the test article.

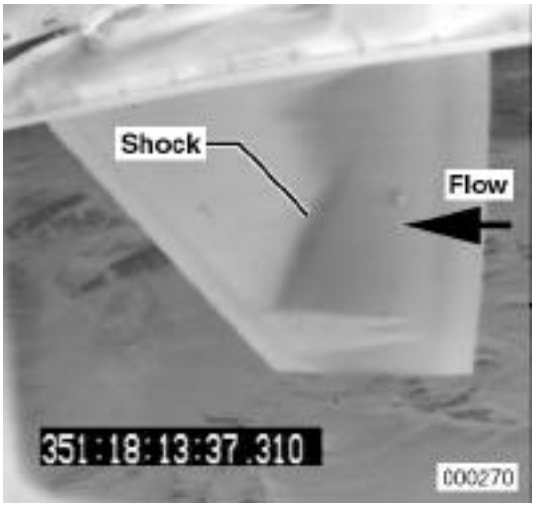

Fig. 8. Example of shock-induced transition at supersonic flight conditions.

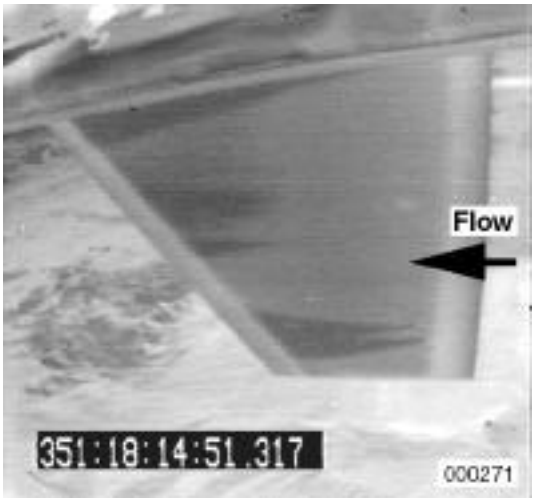

Fig. 9. Warm wall conditions at supersonic flight conditions.

5 SUMMARY OF RESULTS

The use of infrared thermography to visualize a supersonic flow field and define transition boundaries has been demonstrated. In addition to identifying boundary layer transition, the infrared images have been able to identify shock waves impinging on the surface of the test article. Video sequences are able to reveal time dependent processes. The images presented were acquired and stored on Hi-8 tape and later digitized. Once implemented these systems can rapidly acquire data throughout a wide range of flight conditions.

The temperature prediction procedure allows us to evaluate the effects of transient flight conditions, solar heating, and heat conduction, among other phenomena on the surface temperature distribution. The results of these simulations provide insight into the need of, as well as the type and amount of, surface insulation for in-flight infrared imaging. The structural and surface design of the test article is an important consideration for obtaining meaningful data from infrared systems.

Data is currently collected on Hi-8 videotape using the S-video output from the camera. After collection this data is then digitized for further analysis. An upgrade is currently in progress to acquire and store the images digitally. In subsequent tests, the camera's full 12-bit signal would be captured and stored. These digital images would likely provide additional detail of these types of flow fields. The recording system would support continuous collection of digital data for up to two hours. Data collection can be started and stopped using a cockpit control switch. Flight data is downloaded post flight to a portable FireWire hard drive at approximately three times the real time recording rate. The portable drive can be connected to a computer workstation or network for long term storage or analysis. The acquisition of raw digital data would allow more intensive image processing and more detailed flow analysis. Many other aerodynamic phenomena can potentially be visualized using infrared thermography, such as separation or vortical flow, it is only necessary to create a measurable temperature difference that can be differentiated by the sensor.

6 NOMENCLATURE

A	area, m^2
c_f	coefficient of skin friction (based on freestream properties)
c_p	specific heat at constant pressure, J/kg/K
$c_{p,air}$	specific heat at constant pressure of ambient air, J/kg/K
$c_{p,skin}$	specific heat at constant pressure of test subject's skin, J/kg/K
i, j	grid indices in chordwise and normal directions, respectively
k	thermal conductivity, W/m/K
M_∞	freestream Mach number
N	newtons
q''	rate of heat transfer per unit area, W/m^2
q''_{atm}	rate of heat transfer per unit area due to diffuse atmospheric heating, W/m^2
q''_{cond}	rate of heat transfer per unit area due to conduction within test subject, W/m^2
q''_{conv}	rate of heat transfer per unit area due to convection, W/m^2
q''_{rad}	rate of heat transfer per unit area due to radiation from test subject, W/m^2
q''_{sol}	rate of heat transfer per unit area due to solar heating, W/m^2
R	recovery factor
$R_{laminar}$	recovery factor of laminar boundary layer
$R_{turbulent}$	recovery factor of turbulent boundary layer
t	time, sec
T	temperature, K
T_{aw}	adiabatic wall temperature, K
T_w	wall (surface) temperature, K

T_∞	freestream temperature, K
U_∞	freestream velocity, m/sec
V	volume, m^3
x/c	nondimensionalized chord location
α	absorptivity
γ	ratio of specific heats
ε	emissivity
μ	absolute viscosity, kg/m/sec
ρ	density, kg/m^3
ρ_∞	freestream density, kg/m^3
σ	Stefan-Boltzmann constant, $W/m^2/K^4$

7 REFERENCES

[1] Hall, R. M., Obara, C. J., Carraway, D. L., Johnson, C. B., Wright, R. E., Jr., Covell, P. F., and Azzazy, M.: Comparisons of boundary-layer transition measurement techniques at supersonic Mach numbers. *AIAA Journal*, Vol. 29, No. 6, June 1991, pp. 865-879.

[2] Quast, A.: Detection of transition by infrared image technique. *Proceedings of the ICIASF Record*, Williamsburg, VA, June 22-25, Institute of Electrical and Electronics Engineers, New York, 1987, pp. 125-134.

[3] Brandon, J. M., Manuel, G. S., Wright, R. E., and Holmes, B. J.: In-flight flow visualization using infrared imaging. *Journal of Aircraft*, Vol. 27, July 1990, pp. 612-618.

[4] Miley, S. J., van Dam, C. P., Yip, L. P., Willard, P. E., Crowder, J. P., and Wazlavick, R. L.: Slat transition characteristics on the NASA B737-100 aircraft using infrared imaging and hot-film anemometry. *Flow Visualization VII*, J. Crowder (ed.), Begell House, pp. 950-956.

[5] Green, M. J., Budnik, M. P., Yang, L., and Chiasson, M. P.*: Supporting flight-data analysis for space-shuttle orbiter experiments at NASA Ames Research Center*. NASA TM 84345, April 1983.

[6] Van Dam, C. P., Shiu, H. J. and Banks, D. W.: Remote in-flight boundary layer transition visualization using infrared thermography. *8th International Symposium on Flow Visualization*, Sorrento, Italy, 1998.

[7] Blanchard, R. C. and Tietjen, A.: Infrared sensing aeroheating flight experiment (ISAFE). 9th International Symposium on Flow Visualization, Edingburgh, UK, 2000.

[8] Dwyer, H. A., Yam, C., Tang, K., and McKillop, A.: Computational methods in heat transfer; notes for ME165. Department of Mechanical Engineering, University of California, Davis, Davis, California, Fall 1994, pp.37-39.

[9] Drela, M.: Newton solution of coupled viscous/inviscid multielement airfoil flows. AIAA Paper 90-1470, June 1990.

[10] Eckert, E. R. G.: Engineering relations for heat transfer and friction in high-velocity laminar and turbulent boundary-layer flow over surfaces with constant pressure and temperature, *Transactions of the ASME*, Vol. 78, No. 6, August 1956, p. 1273.

[11] Shapiro, A. H.: *The Dynamics and Thermodynamics of Compressible Fluid Flow*. Ronald Press Co., 1953-54.

[12] Mack, L. M.: Boundary-layer stability theory, *Special Course on Stability and Transition of Laminar Flow*, AGARD R-709, June 1984, pp. 3−1-3−81.

[13] Braslow, A. L., and Knox, E. C.: *Simplified method for determination of critical height distributed roughness particles for boundary-layer transition at Mach numbers from 0 to 5*, NACA TN 4363, September 1958.

REPORT DOCUMENTATION PAGE

Form Approved
OMB No. 0704-0188

1. AGENCY USE ONLY (Leave blank)	2. REPORT DATE	3. REPORT TYPE AND DATES COVERED
	July 2000	Technical Memorandum

4. TITLE AND SUBTITLE

Visualization of In-Flight Flow Phenomena Using Infrared Thermography

5. FUNDING NUMBERS

WU 529-35-14-M1-00-38-0-00-S-000

6. AUTHOR(S)

D. W. Banks, C. P. van Dam, H. J. Shiu, and G. M. Miller

7. PERFORMING ORGANIZATION NAME(S) AND ADDRESS(ES)

NASA Dryden Flight Research Center
P.O. Box 273
Edwards, California 93523-0273

8. PERFORMING ORGANIZATION REPORT NUMBER

H-2422

9. SPONSORING/MONITORING AGENCY NAME(S) AND ADDRESS(ES)

National Aeronautics and Space Administration
Washington, DC 20546-0001

10. SPONSORING/MONITORING AGENCY REPORT NUMBER

NASA/TM-2000-209027

11. SUPPLEMENTARY NOTES

Paper no. 24, prepared for the International Symposium on Flow Visualization, August 22–25, 2000, Edinburgh, Scotland. D. W. Banks, NASA Dryden Flight Research Center, Edwards, CA; C. P. van Dam and H. J. Shiu, Dept. of Mechanical and Aeronautical Eng., Univ. of California, Davis, CA; and G. M. Miller, PVP Advanced EP Systems, Orange, CA.

12a. DISTRIBUTION/AVAILABILITY STATEMENT

Unclassified—Unlimited
Subject Category 34

This report is available at http://www.dfrc.nasa.gov/DTRS/

12b. DISTRIBUTION CODE

13. ABSTRACT (Maximum 200 words)

Infrared thermography was used to obtain data on the state of the boundary layer of a natural laminar flow airfoil in supersonic flight. In addition to the laminar-to-turbulent transition boundary, the infrared camera was able to detect shock waves and present a time dependent view of the flow field. A time dependent heat transfer code was developed to predict temperature distributions on the test subject and any necessary surface treatment. A commercially available infrared camera was adapted for airborne use in this application. Readily available infrared technology has the capability to provide detailed visualization of various flow phenomena in subsonic to hypersonic flight regimes.

14. SUBJECT TERMS

Boundary layer transition, Flow visualization, Infrared thermography, Shock waves, Supersonic flow

15. NUMBER OF PAGES

17

16. PRICE CODE

A03

17. SECURITY CLASSIFICATION OF REPORT	18. SECURITY CLASSIFICATION OF THIS PAGE	19. SECURITY CLASSIFICATION OF ABSTRACT	20. LIMITATION OF ABSTRACT
Unclassified	Unclassified	Unclassified	Unlimited